Double-peaked thermonuclear bursts at the soft–hard state transition in the Rapid Burster

T. Bagnoli,[1,2]★ J. J. M. in 't Zand,[1] A. Patruno[3,4] and A. L. Watts[2]

[1] *SRON Netherlands Institute for Space Research, Sorbonnelaan 2, 3584 CA Utrecht, the Netherlands*
[2] *Astronomical Institute 'Anton Pannekoek', University of Amsterdam, Postbus 94249, 1090 GE Amsterdam, the Netherlands*
[3] *Leiden Observatory, Leiden University, PO Box 9513, NL-2300 RA Leiden, the Netherlands*
[4] *ASTRON, the Netherlands Institute for Radio Astronomy, Postbus 2, NL-7990 AA Dwingeloo, the Netherlands*

ABSTRACT

Long suspected to be due to unstable accretion events, the type II bursts exhibited by the Rapid Burster (RB, or MXB 1730−335) still lack an exhaustive explanation. Apart from type II bursts, the transient RB also shows the better-understood thermonuclear shell flashes known as type I bursts. In search of links between these two phenomena, we carried out a comprehensive analysis of all *Rossi X-ray Timing Explorer* observations of the RB and found six atypical type I bursts, featuring a double-peaked profile that is not due to photospheric radius expansion. The bursts appear in a phase of the outburst decay close to the onset of the type II bursts, when the source also switches from the high/soft to the low/hard state. We also report the discovery of a simultaneous low-frequency quasi-periodic oscillation present in the persistent emission as well as in the burst decaying emission. We discuss several scenarios to understand the nature of the peculiar bursts and of the accompanying oscillation, as well as their possible relation with each other and with the type II burst phenomenon. We favour a model consisting of two accretion channels, one polar and one equatorial, in a source viewed at low inclination. We also, for the first time, clearly identify the atoll nature of the RB.

Key words: stars: neutron – X-rays: binaries – X-rays: bursts – X-rays: individual: MXB 1730−335.

1 INTRODUCTION

The Rapid Burster (RB; e.g. Lewin, van Paradijs & Taam 1993) is a transiently accreting neutron star (NS) low-mass X-ray binary (LMXB), with outbursts recurring in less than one year (Masetti 2002) and peak luminosities up to nearly half the Eddington limit (Bagnoli et al. 2013, hereafter B13). It is located in the globular cluster Liller 1, at a distance of 7.9 ± 0.9 kpc (Valenti, Ferraro & Origlia 2010). It is unique, in that it shows both type I bursts, which are X-ray eruptions due to the heating and cooling of the NS photosphere after a thermonuclear shell flash of accreted material (see e.g. reviews by Strohmayer & Bildsten 2006 and Galloway et al. 2008), and type II bursts, most likely due to the release of gravitational energy during sudden accretion episodes (Hoffman, Marshall & Lewin 1978). While the former are relatively well understood and observed in over a hundred sources, it remains unclear why the latter have been unambiguously detected in only two NS LMXBs, the other one being the slowly rotating (2 Hz) Bursting Pulsar (Kouveliotou et al. 1996).

The Proportional Counter Array (PCA) onboard the *Rossi X-ray Timing Explorer* (*RXTE*) observed 125 type I and about 7050 type II bursts from the RB. A complete analysis (B13) of the type I burst sample shows that type I bursts appear in the RB over a remarkably large range of mass accretion rates, recurring faster as its bolometric luminosity increases to a large fraction of the Eddington limit, a behaviour only shared with the 11 Hz pulsar IGR J17480−2446 (Linares et al. 2012) among over a hundred bursting LMXBs (see e.g. Cornelisse et al. 2003). The known NS spin frequencies in these systems range between 245 and 620 Hz (Watts 2012), and the exceptional bursting behaviour of IGR J17480−2446 can be explained only thanks to its slow NS spin (Linares et al. 2012). This indicates the RB should be a slow rotator too (B13).

Type II bursts instead appear only after the outburst has significantly decayed, usually below a bolometric persistent flux of $F_{\rm pers} \approx 3 \times 10^{-9}$ erg cm^{-2} s^{-1} (Guerriero et al. 1999). They often show a relaxation-oscillator behaviour, meaning that the fluence in a type II burst is proportional to the waiting time to the next one. These properties hint at disc-magnetosphere interactions that are largely thought to control the type II burst phenomenon (Baan 1977, 1979; Lamb et al. 1977; Spruit & Taam 1993). Type II bursts in the RB are often accompanied by low-frequency quasi periodic oscillations (LF QPOs) in the persistent emission, both at frequencies ν_0 between 2 and 4 Hz, and at much slower values centred about an average of 42 mHz. They both cease right before the onset of a type II burst, so it is likely that they originate in the same mass

★ E-mail: t.bagnoli@sron.nl

reservoir whose spasmodic accretion is responsible for the type II burst (Stella et al. 1988; Lubin et al. 1992).

Much theoretical work (e.g. Kulkarni & Romanova 2008; D'Angelo & Spruit 2010, 2012; Romanova et al. 2012) has focused on the dynamical role of the magnetic field, which can act as a 'gating' mechanism to the accretion flow once the mass accretion rate drops below a certain threshold. These models could explain the episodic accretion that is responsible for the type II burst phenomenon, but also LF QPOs at low-mass accretion rates, as those observed in the light curves of the accreting millisecond X-ray pulsars (AMXPs) SAX J1808.4−3658 (Patruno et al. 2009) and NGC 6440 X-2 (Patruno & D'Angelo 2013).

We report here on six peculiar type I bursts that stand out among the RB PCA sample because of a unique double-peaked structure first noticed by Fox et al. (2001). We show that four of these bursts appear at the transition from the high/soft to the low/hard state (van der Klis 2006), and that this takes place at the time of the first appearance of type II bursts. We exclude the possibility that their double peaks are due to photospheric radius expansion (PRE; see e.g. Lewin et al. 1993). We also find a previously unreported QPO at a frequency of about 0.25 Hz. The QPO becomes visible in the persistent emission a few days before the double-peaked bursts, peaks in amplitude at the time the bursts appear, even becoming directly visible in the light curve, and fades out over the next few days.

We describe the spectral and timing properties of the double-peaked type I bursts and the LF QPO accompanying them, and investigate whether they can shed further light on the nature of the interaction between accretion and magnetic-field effects in the enigmatic RB. Section 2 describes the data set and discusses the data analysis. Section 3 presents the results of our analysis, and finally Section 4 discusses the interpretation of these results in the context of models and observations of other sources.

2 OBSERVATIONS

Most measurements described here were obtained through observations with the PCA. The PCA (Jahoda et al. 2006) is a non-imaging system consisting of five co-aligned proportional counter units (PCUs) that combine to a total effective area of 6500 cm^2 at 6 keV, in a 2 to 60 keV bandpass. The photon energy resolution is 18 per cent full width at half-maximum (FWHM) at 6 keV and the time resolution is programmable down to about 1 μs. The field of view (FOV) is approximately circular, with radius 1° (full width to zero response). The *RXTE* observations of the RB include a mix of data. There are observations directly pointed at the source that are contaminated by the presence of 4U 1728−34 at an angular distance of 0°.56 (Galloway et al. 2008), and offset pointings that do not suffer from such contamination, albeit at the price of a smaller effective area. The total exposure time obtained on the RB while it was active is 0.91 Msec. For further details on source confusion in the FOV, burst identification and discrimination between type I and type II bursts, we refer the reader to B13.

Six type I bursts have a peculiar double-peaked time profile. They are numbered 35, 36, 37, 58, 118 and 119, following their chronological position among the 125 type I burst in the PCA sample (B13). Three of the six double-peaked type I bursts subject of this paper occurred during one outburst which is shown in Fig. 1. The burst light curves (Fig. 2) were constructed employing 0.125 s resolution STANDARD 1 data. Typically, type I X-ray bursts of the RB show a two-component decay profile, with a steeper 10 s long initial decay and a shallower 100 s long tail, whose relative
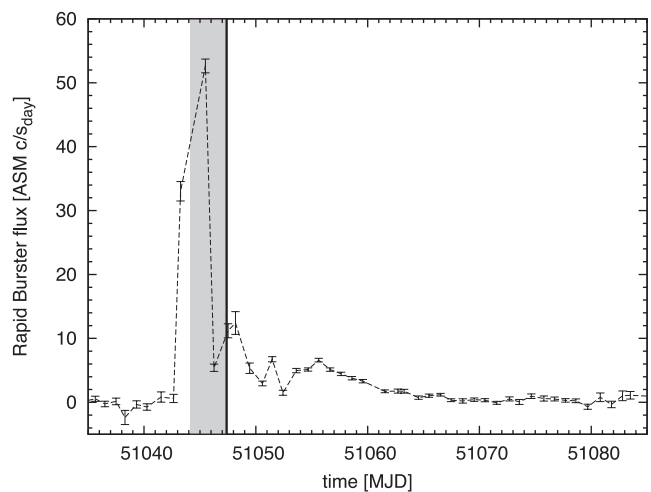
Figure 1. Daily average 3–12 keV flux of the RB measured with the All-Sky Monitor (ASM, Levine et al. 1996) on board the *RXTE* during the 1998 August–September outburst. The three double-peaked type I bursts 35 through 37 occur within ≲2 h (thick black line). The 0.25 Hz QPO (see Section 3.3) is visible in the power spectra for about three days, from the beginning of the PCA observations until the double-peaked bursts (grey-shaded area). Long, flat-topped and very energetic type II bursts appear at the same time (see Section 3.1).

amplitude varies (B13). We constructed an average type I burst profile employing 22 bursts which we chose because they show the longest and brightest decays. This average burst profile is plotted against each burst in Fig. 2.

We define a few variables to help us quantify the morphology of the dip between the peaks. First, we applied an exponential fit to the first 200 s of the slow-decay portion of the burst after the second peak. We extrapolated this fit backwards to determine the time $t_{\rm dip, start}$ when it intercepts the first peak of the burst. The dip duration $\Delta t_{\rm dip}$ is the time between $t_{\rm dip,start}$ and the time of the second peak. The dip depth D is the ratio of the number of photons lacking under the extrapolated curve during the interval $\Delta t_{\rm dip}$ over the total number of observed photons between the burst start- and end times (defined as in B13).

Time-resolved spectroscopy of the burst data was performed following the same procedure and tools as in B13. The particle and cosmic background were determined with FTOOL PCABACKEST and subtracted from all spectra. Response matrices were generated with PCARSP (v. 11.7.1). All active PCUs were employed, and a correction was applied for deadtime (although it is always small for the RB). Following the *RXTE* Cookbook prescription,[1] the analysis was limited to the 3–25 keV range, and a systematic error of 0.5 per cent was added in quadrature to the statistical error of the flux in each channel. The burst data were divided into a number of time bins, varying in duration to keep the photon count, and hence the relative error on the derived quantities, approximately constant.

3 RESULTS

3.1 The outbursts

Typical RB outbursts observed by *RXTE* prior to 1999 November tend to have a fast rise of 1 to 3 d, followed by an exponential

---

[1] See http://heasarc.nasa.gov/docs/xte/recipes/cook_book.html
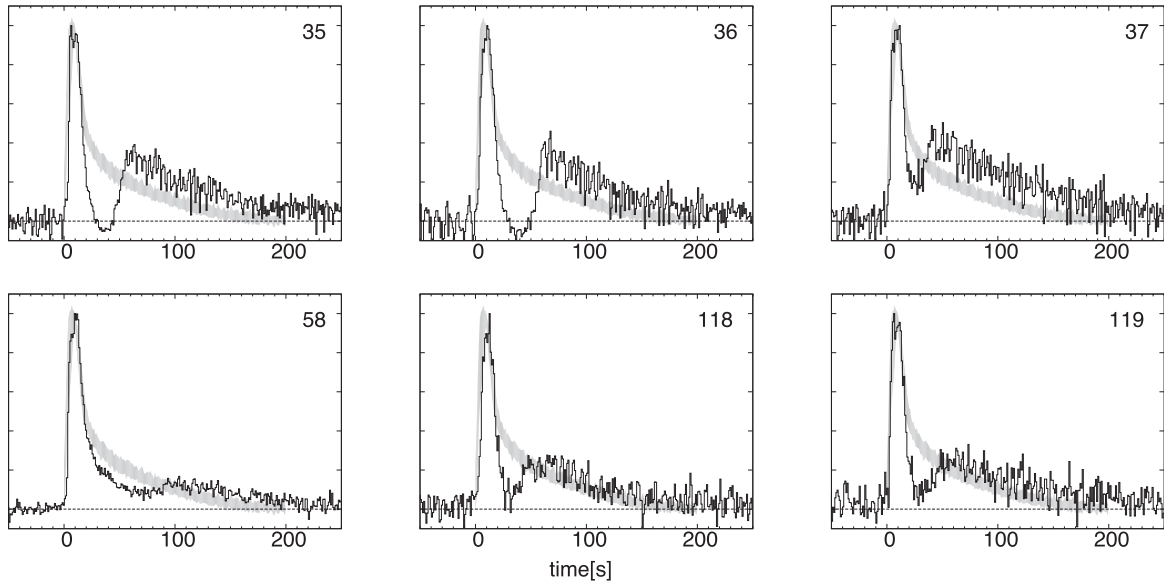
Figure 2. The six bursts studied here. The time axis has been shifted so that at the burst start time $t = 0$. The subtracted background level is measured from a 500 s time interval prior to the burst. The curves are normalized to their individual peak rate. The zero level is indicated by a dashed line. Each burst is plotted against the average profile of the 22 single-peaked type I bursts featuring the longest and brightest decays (see Section 3.2). The shaded region indicates the standard deviation of the sample. The large oscillations in the decays of bursts 35 through 37 are not due to random (white) noise, but to the 0.25 Hz QPO. They are clearly still visible in the shallower dip of burst 37, but absent in the deeper dip of burst 35. Burst 58 reaches a much larger count rate in its first peak, which makes the second peak and the QPO harder to see in this scaling.

decay with an e-folding decay time of about 8 d. Initially only type I bursts are observed. Type II bursts activity starts about 18 d into the outburst, when typically the bolometric flux decreased to a level of $F_{\rm pers} \approx 3 \times 10^{-9} \, {\rm erg \, cm^{-2} \, s^{-1}}$. The first type II bursts to appear (the so-called mode-0 type II bursts) are long (200–300 s), bright (up to 3000 c s^{-1} PCU^{-1}), flat-topped and short-lived, usually being visible for only a couple of days. We inspected all the light curves visually and only found 18 mode-0 type II bursts. Their rarity is due both to the short outburst fraction in which they are produced and to their long recurrence time, which for RB type II bursts is proportional to the fluence in a burst (the so-called relaxation-oscillator behaviour, Lewin et al. 1993). Shorter, more frequent (the so-called mode I and mode II) type II bursts then follow for another couple of weeks until the end of the outburst (Guerriero et al. 1999).

The 1998 August–September outburst during which bursts 35 through 37 appeared has an atypical light curve shape (see Fig. 1), featuring a much faster decay, as well as much earlier mode-0 type II bursts, which could have started already during the outburst rise (Fox et al. 1998). Although no PCA coverage is available for more than three days before, the timing of the three double-peaked bursts seems also quite interesting. As can be seen in Fig. 1, these double-peaked bursts occur during the initial phase of type II bursts, at a time when the source is experiencing rapid and large variations in flux ('reflares'). These considerations make us confident that the peculiar sequence of double-peaked type I bursts occurs close to the onset of the type II bursting activity.

Burst 58 was observed eight days after the start time of the PCA observations of the 1999 October outburst. In the time leading to it, 12 type I bursts are observed, and no type II bursts. No observation is available in the three days prior to burst 58, and not again until four days later. Short (mode-I) type II bursts are first observed 10 d after burst 58. It seems plausible that this could be a more typical outburst, and that the short-lived phase of strong, long and flat-topped (mode-0) type II bursts was missed

because of the rather limited coverage around the time it could have occurred.

Bursts 118 and 119 took place during the last RB outburst observed by *RXTE*, in 2010 January. Less than 12 ks of PCA data are available for this outburst, in five observations spanning only 3 d. It is therefore difficult to assess to what extent the outburst has already decayed when these bursts occur. However, starting in 2000 all outbursts recurred within a shorter time and peaked at significantly lower intensities (Masetti 2002). Therefore, the initial type-I-only phase of the outburst can be significantly shorter. Judging from the All-Sky Monitor light-curve, bursts 118 and 119 occurred no longer than 2 d after the beginning of the outburst. None the less, the presence of six more type I bursts, the burst recurrence time (see Section 3.2.1), the count rate in the persistent emission and the lack of type II bursts are all consistent with what is observed in the other four double-peaked bursts, which indicates a similar accretion state.

3.2 The double-peaked bursts

3.2.1 Light curves

Fig. 2 shows the six double-peaked type I bursts under analysis and Table 1 lists their characteristics. Bursts 35 through 37 occurred with a recurrence time of about 2.2 ks, which is in the middle of the range of observed values of all RB type I bursts (B13). In bursts 35 and 36, the dip clearly lasts longer ($\Delta t_{\rm dip} = 46$ s) and the flux even drops to about 5 per cent below the pre-burst emission level. The dip in burst 37 is instead shorter, at 25 s, and the flux only drops to about 20 per cent of the net burst peak count rate. While the QPO is not visible during the dips of bursts 35 and 36, it is still present in that of burst 37.

The second peak is about 40 to 50 per cent as large as the first one. It is higher in burst 37, where it occurs earlier. The QPO modulation is clearly visible again in the second portion of the decays.

Table 1. Properties of the double-peaked bursts.

Burst	Obs ID	$F_{\text{peak},1}^{(a)}$ $(10^{-9}\,\text{erg}\,\text{cm}^{-2}\,\text{s}^{-1})$	$F_{\text{peak},2}^{(b)}$ $(10^{-9}\,\text{erg}\,\text{cm}^{-2}\,\text{s}^{-1})$	$E_{\text{b}}^{(c)}$ $(10^{-8}\,\text{erg}\,\text{cm}^{-2})$	$E_{\text{sf}}/E_{\text{b}}^{(d)}$	$\Delta t_{\text{dip}}^{(e)}$ (s)	$D^{(f)}$
35	30079-01-03-00R	6.0 ± 0.5	2.3 ± 0.6	23.4 ± 1.1	(35 ± 6) per cent	46	44 per cent
36	30079-01-03-00R	5.7 ± 0.4	1.8 ± 0.4	20.7 ± 1.1	(34 ± 7) per cent	46	56 per cent
37	30079-01-03-01R	5.9 ± 0.5	2.7 ± 0.6	28.8 ± 1.7	(31 ± 9) per cent	25	11 per cent
58	40433-01-02-00R	9.5 ± 0.5	1.1 ± 0.3	29.9 ± 1.5	(73 ± 7) per cent	72	26 per cent
118	95410-01-01-00	5.2 ± 0.8	1.2 ± 0.3	17.1 ± 1.9	(28 ± 6) per cent	33	17 per cent
119	95410-01-01-00	5.4 ± 0.8	1.2 ± 0.3	19.1 ± 2.1	(26 ± 4) per cent	30	16 per cent

All fluxes and fluences are bolometric. $^{(a)}$ First-peak flux. $^{(b)}$ Second-peak flux. $^{(c)}$ Burst fluence. $^{(d)}$ Fractional fluence before the dip. $^{(e)}$ Dip duration. $^{(f)}$ Dip depth, the fraction of photons lost to the dip. See Section 2 for explanation.

Looking at Fig. 2, it is clear that the post-dip portion of the decay is significantly brighter than in the rest of the type I bursts sample. As a result, the bursts are also longer. If however one only looks at the minima of the QPO, the decays might have durations comparable to those observed in the rest of the sample.

Burst 58 has a much dimmer second peak with respect to the other bursts, only about 15 per cent above the net burst count rate, which is however still significantly above the persistent emission. It features the longest dip, at $\Delta t_{\text{dip}} = 72$ s, going down to just about 4 per cent above the persistent emission, but still significantly above the noise fluctuations.

The recurrence time for bursts 118 and 119 is 1.8 ks, similar to what is observed for bursts 35–37. Their dips are about 30 s long, and briefly drop to count rates within 1 per cent of those observed right before the bursts. Like in burst 37, the QPO remains visible during the dip. Their second peaks are about 30 per cent as large as the first ones.

3.2.2 Spectral properties of the pre-burst emission

Burst 35 and 36 were observed during a direct pointing, while burst 37 took place in an offset configuration (see Section 2). The pre-burst spectrum of the RB was derived from the available 182 s-long segment of the light curve prior to burst 37. We fitted this with a model that is a good description of all RB non-burst data (B13) and consists of a disc blackbody (Mitsuda et al. 1984), a power law and a Gaussian line at 6.4 keV. Low-energy absorption by the interstellar medium was taken into account using the model of Morrison & McCammon (1983), with an equivalent hydrogen column density of $N_{\text{H}} = 1.6 \times 10^{22}\,\text{cm}^{-2}$ (Frogel, Kuchinski & Tiede 1995; Masetti et al. 2000; Falanga et al. 2004). The resulting blackbody temperature is (2.48 ± 0.06) keV, the apparent disc radius (1.77 ± 0.06) km $\times$ $(D/10\,\text{kpc})/\sqrt{\cos i}$ (with D the source distance and i the disc inclination; for the relation between the apparent and realistic inner disc radius, see Kubota et al. 1998) and the power-law photon index is 2.35 ± 0.23. The goodness of the fit is $\chi_{\text{red}}^2 = 1.25$ for 46 degrees of freedom (d.o.f.). We call this the 'RB spectrum'.

For the persistent emission prior to bursts 35 and 36, whose observations are contaminated by the nearby source 4U 1728−34, which dominates above 20 keV, simply renormalizing the RB spectrum according to the collimator responses (1.0 and 0.42 for the on- and offset pointings, respectively) while leaving the other parameters frozen (under the assumption that the spectrum does not change significantly over the short time separating the observations) yields unacceptable fits [for burst 35, $\chi_{\text{red}}^2(\text{d.o.f.}) = 53.2(51)$]. We therefore also added an absorbed Comptonization model ($N_{\text{H}} = 2.4 \times 10^{22}\,\text{cm}^{-2}$; Egron et al. 2011), which we refer to as the

'4U 1728−34 spectrum'. This fit gave $\chi_{\text{red}}^2(\text{d.o.f.}) = 1.10(46)$ and $1.04(46)$ for the persistent-emission spectrum before bursts 35 and 36, respectively.

Analogously, a persistent emission spectrum was extracted from an offset pointing 1200 s after burst 58, corrected for the collimator response, and added to a component describing 4U 1728−34, for an overall good fit with $\chi_{\text{red}}^2(\text{d.o.f.}) = 0.85(42)$. Finally, no offset observations were available near bursts 118 and 119. Therefore, we simply fit a model similar to the one described above (an 'RB' plus a '4U 1728−34' component) to each of their pre-burst spectra, which gave $\chi_{\text{red}}^2(\text{d.o.f.}) = 0.63(49)$ and $0.88(49)$, respectively.

3.2.3 Spectral properties of the bursts

Spectra during the bursts were modelled by the combination of blackbody radiation (leaving free temperature and emission area, to account for the varying burst emission, and multiplied by a model for interstellar absorption with $N_{\text{H}} = 1.6 \times 10^{22}\,\text{cm}^{-2}$) and the model as found for the non-burst spectrum discussed above, keeping the parameters of the latter fixed. The spectral properties of the bursts are listed in Table 1.

Bursts 35 to 37 reach remarkably similar bolometric peak fluxes F_{peak} (in units of $10^{-9}\,\text{erg}\,\text{cm}^{-2}\,\text{s}^{-1}$), from 5.7 ± 0.4 to 6.0 ± 0.5 in the first peak, while ranging from 1.8 ± 0.4 to 2.7 ± 0.6 in the second one. Burst 58 has instead a 50 per cent brighter first peak, at $F_{\text{peak}} = 9.5 \pm 0.5$, and a dimmer second peak, at 1.1 ± 0.3. Finally, bursts 118 and 119 have bright first peaks, comparable to those of bursts 35–37, and dim second peaks like that of burst 58. Such fluxes are all significantly sub-Eddington: for the quoted distance, the Eddington flux is $F_{\text{Edd}} = 2.1 \times 10^{-8}\,\text{erg}\,\text{cm}^{-2}\,\text{s}^{-1}$ for a 'canonical' NS with mass $M = 1.4\,\text{M}_\odot$ accreting solar-composition material (hydrogen fraction $X = 0.7$).

The total burst fluence E_{b} spans from $(17.1 \pm 1.9) \times 10^{-8}\,\text{erg}\,\text{cm}^{-2}$ to $(29.9 \pm 1.5) \times 10^{-8}\,\text{erg}\,\text{cm}^{-2}$. Despite its brighter first peak, burst 58 is not more energetic than burst 37. This is again because there are differences in how the energy is distributed before and after the second peak: in bursts 35–37, 118 and 119, 27 to 35 per cent of the fluence is emitted before the dip, and 65 to 73 per cent after it. In burst 58 instead, 73 per cent of the fluence is emitted up to the dip minimum and only 27 per cent after it.

The results of the time-resolved spectroscopic analysis for burst 35 are plotted in Fig. 3. Two main conclusions can be drawn. First, a decreasing temperature accompanied by an increasing radius while the flux drops out of the instrumental bandpass, the hallmarks of photospheric expansion (see e.g. Galloway et al. 2008), are not visible in the spectral evolution. This is also true during the other dips. Therefore, we conclude that they are not due to PRE.
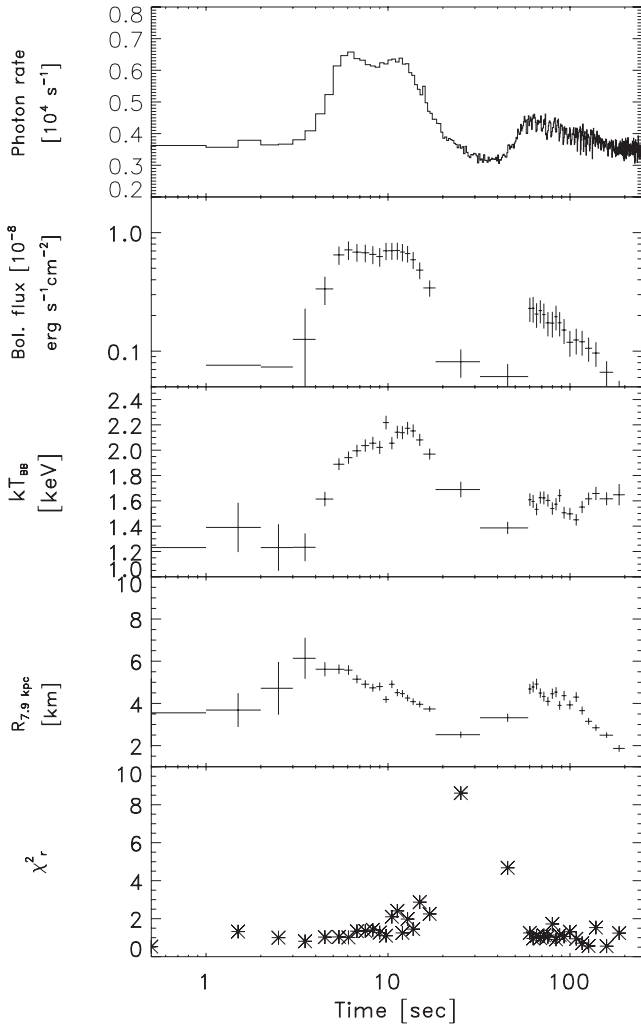
Figure 3. Time-resolved spectroscopy of burst number 35. The top panel shows the measured full-bandpass photon count rates for the PCA Xenon layers. Following downward, the bolometric flux, the blackbody temperature and radius (assuming a distance of 7.9 kpc) and the χ^2_{red} of the fit are plotted. It is clear that no PRE takes place, and that during the dip the pre-burst spectrum yields an unacceptable fit (see Section 3).

Secondly, the goodness of fits worsens during the decay into the dips of bursts 35 and 36, until χ^2_{red}(d.o.f.) becomes as large as 8.5(27) and 4.2(26), respectively, when the count rate is roughly at the pre-burst level. We therefore examined whether the spectrum in these dips is different from that in the persistent emission prior to the burst.

We attempted to fit the dip spectrum of burst 35 with three different models. The spectrum was extracted between 32 and 40 s after the burst start, when the flux is stable at about 5 per cent below the count rate of the persistent emission prior to the burst (see Fig. 2). The model that fitted the pre-burst emission (see Section 3.2.2) was unacceptable for the burst dip, with χ^2_{red}(d.o.f.) = 6.68(29). Letting the two additive components that make up the persistent emission (the RB and 4U 1728−34 spectra) free to vary in normalization also yielded an unacceptable fit, with χ^2_{red}(d.o.f.) = 4.18(27). This means that the fit cannot be improved by simply allowing the normalization of the subtracted pre-burst spectrum vary, as successfully done by Worpel, Galloway & Price (2013) for PRE bursts. The energy dependence of the ratio of the model to the data rather suggests

that the discrepancy results from an intrinsically different spectral shape.

We therefore fitted the dip by keeping the 4U 1728−34 spectrum frozen and leaving free to vary different components of the RB spectrum. The only solution with an acceptable fit required a column density $N_H = (6.86 \pm 0.96) \times 10^{22}$ cm^{-2}, more than four times larger than the quoted value, which we normally employ for the pre-burst emission. The required blackbody temperature and radius were (2.03 ± 0.06) keV and (2.55 ± 1.04) km. This choice gave the best-fitting model, with χ^2_{red}(d.o.f.) = 1.28(26). Conversely, it was not applicable to the pre-burst emission, where it yielded χ^2_{red}(d.o.f.) = 96.4(52).

As a final test, we extracted the spectrum of the persistent emission 1000 s after the burst start. In this stretch of data, the count rate is on average 2.5 per cent below the pre-burst emission. We tried to fit the spectrum of this post-burst emission with both the model for the pre-burst emission and for the dip, letting the 'RB spectrum' free to vary in normalization while freezing all the other components. The pre-burst model gave χ^2_{red}(d.o.f.) = 1.32(51) with a normalization 4.2 per cent lower, while the model that best fit the dip resulted in a χ^2_{red}(d.o.f.) = 79.07(51), with a 2.5 per cent higher normalization.

Therefore, the dip has a truly different spectral shape than both the pre- and post-burst emission, even though they are roughly at the same count rate.

3.3 Timing analysis

A timing analysis of a data set which included the double-peaked bursts 35 through 37 was already performed by Fox et al. (2001). However, their main focus was the search of high-frequency burst oscillations, and they calculated Fourier transforms of 1 s long data stretches, thereby ignoring the entire sub-Hz portion of the power spectrum.

For the timing analysis, we used all Good Xenon and Event data, with a time resolution of 2^{-20} and 2^{-13} s, respectively. The Good Xenon data were rebinned to the same resolution as the Event data. No background subtraction or dead-time correction was applied to the data before calculating the power spectra, but type I and II bursts were removed. Following a well-established procedure (see e.g. Klein-Wolt, Homan & van der Klis 2004), we determined the Poisson noise using the formula by Zhang et al. (1995) and then shifted it to the featureless level between 3072 and 4096 Hz, a region in the power spectra dominated by photon counting noise. This mean value was then subtracted from the power spectra. The background was calculated for each observation (Obs ID) with the FTOOL PCABACKEST over the entire energy range. We used 128 s long segments to calculate power spectra with no energy selection. The frequency boundaries for the power spectra are therefore 1/128 Hz and 4096 Hz. The power spectra were normalized to the relative rms (van der Klis 1995) which yields the power density in units of (rms/mean)^2 Hz^{-1}.

We scanned all the PCA power spectra. Each power spectrum was inspected by eye to look for the presence of the LF QPO. When it is present, we fit the logarithmically sampled low-frequency ($\nu < 30$ Hz) portion of the spectrum with a sum of Lorentzian components, following Belloni, Psaltis & van der Klis (2002). Each Lorentzian peaks at a frequency

$$\nu_{max} = \nu_0 \sqrt{1 + \frac{1}{4Q^2}}, \qquad (1)$$
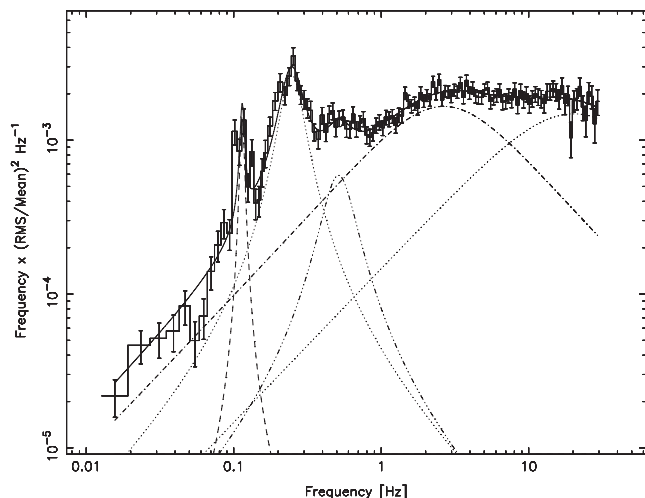
Figure 4. Logarithmically rebinned, power spectrum distribution of all the non-burst data in Obs ID 30079-01-03, which features bursts 35 to 37. Note the QPOs at 0.1 and 0.25 Hz. This is the only detection of the former feature and the most significant detection of the latter. The first harmonic of the 0.25 Hz QPO is also visible at 0.5 Hz.
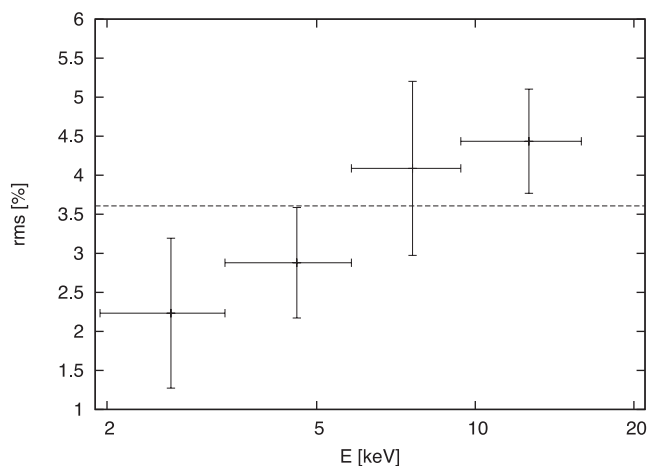
Figure 5. The energy dependence of the ~0.25 Hz QPO, over the same data stretch as covered by Fig. 4. The rms increases with energy. The plot show rms amplitudes up to 17 keV, where counts yield acceptable fits to the feature. Error bars correspond to 1σ levels, the dashed line shows the average rms over all energies.

with centroid frequency ν_0 and coherence factor Q corresponding to the ratio of ν_0 to the FWHM. An example of these fits can be seen in Fig. 4. We then integrated the fractional rms of each Lorentzian over the whole frequency range, and over smaller energy bands, to quantify the energy dependence of the rms (see Fig. 5). Table 2 lists all observations in which the 0.25 Hz QPO was found, and the QPO properties.

We detect the QPO in five distinct Obs IDs, across five different outbursts. They all feature either double-peaked type I bursts or the kind of type II bursts (long, bright, flat-topped) which are the first to appear and are only present in a short phase of an outburst decay (see Section 3.1). The count rates vary by a factor of 2 across these observations. The fits yielded acceptable $\chi^2_{\rm red}$(d.o.f.), varying between 0.92(118) and 1.19(108), across the different observations. The significance of the detection, defined as the ratio of

the integrated power over its negative error varies between 5.33 and 16.64 σ.

The power spectrum of the observation which includes bursts 35 through 37 is shown in Fig. 4. This is the most significant detection of the 0.25 Hz QPO. Besides the main feature an accompanying QPO is visible at 0.1 Hz. Also present are QPOs that peak at 0.5 and 3 Hz, which are known to appear in the run-up to a large type II burst (Stella et al. 1988). The former is probably in a harmonic relation to the 0.25 Hz QPO.

Our newly discovered QPO, relatively well fit by a Lorentzian, covers a relatively narrow frequency range in the different observations, between 0.18 and 0.26 Hz. Its rms amplitude varies between (1.91 ± 0.83) to (5.03 ± 1.47) per cent. At its peak, it is also clearly observed in the time domain (see Fig. 2). As can be seen in Fig. 5, the amplitude seems to grow monotonically over the 2–17 keV (channels 5-64 of the PCA) energy range. The error bars are however quite large, and a constant value could also fit the rms-E relation. We performed an F-test to compare the fits for a constant value and a linear dependence on energy. The linear function yields a better fit, and the probability of the improvement being due to random chance is $p = 0.04$. We therefore consider the growing trend real. The coherence factor Q is rather low, between 0.43 and 2.29. However, we must stress that the feature is sometimes observed to increase in frequency during the intensity decrease that precedes the longest type II burst. This degrades its coherence in our fit, which is averaged over an entire observation.

The weaker 0.1 Hz QPO feature was only detected on the same date as the double-peaked bursts 35–37, while it is not present in the other power spectra, and it is poorly fit by a Lorentzian. Therefore, we cannot establish whether it might be in a harmonic relation with the 0.25 Hz oscillation, nor can we exactly quantify its amplitude or coherence. It is however quite a narrow feature, and it seems weaker than the 0.25 Hz QPO.

We did not fit the power spectra of the remainder of the observations, but a visual inspection of the power spectra indicated that the QPO disappears as the rare, 300 s long, flat-topped type II bursts (which are the first to appear in an outburst, Guerriero et al. 1999) evolve into shorter, more frequent ones at lower count rates.
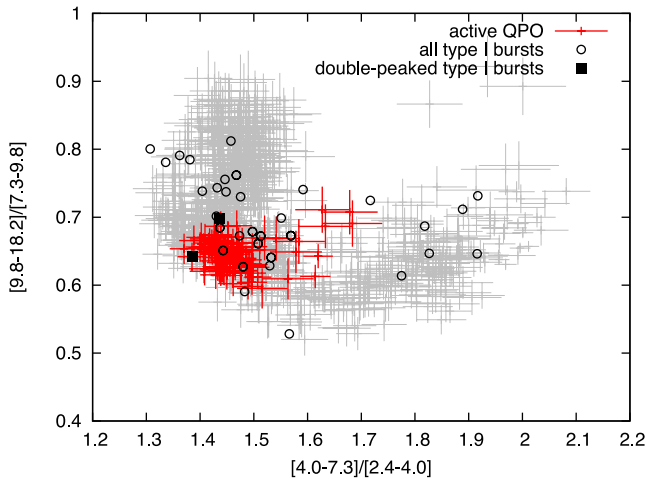
3.4 The colour–colour diagram

There are $\simeq$335 ks of non-contaminated exposures with 4U 1728−34 outside the FOV and the active RB inside. We employed 16 s time resolution STANDARD 2 data for these observations to calculate X-ray colours.

Following Homan et al. (2010), soft and hard colours are defined as the ratio of counts in the $\simeq$4.1–7.3 keV to that in the $\simeq$2.5–4.1 keV band, and in the $\simeq$9.8–18.1 keV and $\simeq$7.3–9.8 keV bands, respectively. Type I and II bursts were removed, background was subtracted, and dead-time corrections were made. The energy-channel conversion was determined from the pca_e2c_e05v01 table provided by the *RXTE* team. In order to correct for gain changes as well as for differences in effective area between the PCUs, we normalized our colours to the corresponding Crab source colour values (van Straaten, van der Klis & Méndez 2003) that are closest in time and in the same *RXTE* gain epoch, to make sure the same high-voltage settings of the PCUs apply. Continuous stretches of data points were combined until the relative error of each colour was below 5 per cent. Finally, we flagged the colours closest in time to the double-peaked bursts 37 and 58. The former measurement is also very close to bursts 35 and 36. Bursts 118 and 119 have no close-by non-contaminated exposure.

Table 2. Log of the *RXTE* timing measurements of the RB power spectral fit parameters.

Obs ID	Date	Start time (UTC)	t_{obs} (ks)	rms (per cent)	Q	ν_0 (Hz)	Significance σ	Count rate (c s^{-1} PCU^{-1})
30079-01-03[a]	1998 Aug 22	08:10:36	8.7	$3.93^{+0.95}_{-0.97}$	2.29 ± 0.21	0.25 ± 0.004	16.64	569
40058-02-03	1999 Mar 19	18:12:43	17.2	$1.91^{+0.84}_{-0.82}$	1.42 ± 0.43	0.20 ± 0.016	5.33	320
40433-01-02[b]	1999 Oct 08	12:06:23	3.0	$2.28^{+0.67}_{-0.63}$	0.43 ± 0.13	0.20 ± 0.017	12.13	555
50420-01-09	2001 Feb 16	14:12:45	11.7	$5.03^{+1.47}_{-1.48}$	0.79 ± 0.10	0.26 ± 0.011	11.68	266
95410-01-01[c]	2010 Jan 15	20:41:33	2.8	$2.61^{+1.06}_{-1.11}$	2.01 ± 0.66	0.18 ± 0.006	5.74	405

Errors on the parameters were determined using $\Delta\chi^2 = 1$. [a]Includes bursts 35 to 37. [b]Includes burst 58. [c]Includes bursts 118 and 119.

Figure 6. Colour–colour diagram (CCD) of the RB. Circles indicate colours of the persistent emission as close to a type I burst as possible, filled squares indicate the same but for four double-peaked bursts. The red data points refer to the data where the QPO is observed. While ordinary type-I bursts take place in all source states, the double-peaked bursts and the 0.25 Hz QPO are only visible at the vertex between the island and banana branches. Offset observations were chosen, for a total of 335 ks, so that 4U 1728−34 is not contaminating the FOV of the PCA, and type I and II bursts were removed from the data. Each data point represents 16 s of data. Where needed, the data were binned in time, to keep errors on each colour below 5 per cent.

Fig. 6 shows the resulting colour–colour diagram (CCD). Two clearly distinct branches are present which indicate that the RB is an atoll source, with the so-called banana and island states (Hasinger & van der Klis 1989). Type I bursts take place in a wide range of mass accretion rates, as already shown by B13. Interestingly, the double-peaked bursts and the accompanying 0.25 Hz QPO concentrate at the vertex where the RB transits from the lower banana to the island state.

4 DISCUSSION

4.1 Observational summary

In a comprehensive analysis of all *RXTE* data on the RB, we found six type I X-ray bursts during three outbursts that feature a dip that is not due to PRE, resulting in the appearance of two peaks in the light curves. The dips are relatively long with durations between 25 and 72 s and ingresses and egresses that have a typical time-scale of 10 s. In two bursts, the dips drop for about 10 s below the pre-burst flux level, by up to 5 per cent. The dip is therefore also in the persistent emission, although never outside a burst. When that

happens, the spectral shape is different from the pre-burst spectrum with an increase of the absorption column density by a factor of 4. After the burst, the persistent emission recovers its pre-burst spectral shape. Such a peculiar and repetitive morphology of type I burst light curves has, to the best of our knowledge, never been observed before (see Section 4.2).

With respect to the other type I bursts from the RB, the duration of the double-peaked bursts seems longer and the decays after the second peak brighter, but that may be due to the addition of the QPO on the tail and not on the first peak. The fluence of the bursts ranges between 17.12 and 28.80 × 10^{-8} erg cm^{-2}. This compares with 17.6 to 51.5 × 10^{-8} erg cm^{-2} for the other 121 bursts (B13). If the dips hide part of the actual fluence, the total fluence would be between 10 and 50 per cent larger, varying between about 20 and 37 × 10^{-8} erg cm^{-2}. Instead, the pre-dip fluence alone is between 4.80 and 9.01 × 10^{-8} erg cm^{-2} which is significantly below the lowest value for all other bursts. These ranges are a strong indication that the second peaks are thermonuclear in nature and not, for instance, completely due to accretion. The other burst properties, like peak flux, rise and recurrence times are quite unremarkable compared to the rest of the sample. However, it must be noted that the recurrence time of the bursts spans a rather limited range, between 1.7 and 2.2 ks, and that they appear at similar persistent count rates. B13 showed that the RB produces bursts over a very large range of persistent fluxes, and that the recurrence time-scales accordingly. It seems therefore likely that the double-peaked bursts are peculiar to a limited range of mass accretion rates.

RXTE data of the RB suffer from contamination of another bright LMXB in the same FOV: 4U 1728−34. This does not affect the analysis of X-ray bursts since those of the RB are easily discerned from those of 4U 1728−34, but the analysis of the non-burst radiation is seriously affected, which precluded thus far the identification of the RB as an atoll or Z-source (Rutledge et al. 1995). However, a portion of the observations were pointed such that 4U 1728−34 is outside the FOV, while the RB remains inside, though at a less favourable off-axis angle. Thanks to the large size of the data set collected by *RXTE* during its mission, we generated a CCD from these data and are able, for the first time, to identify the RB as an atoll source with unambiguous 'island' and 'banana' branches (Hasinger & van der Klis 1989).

The double-peaked bursts seem to occur at a phase in the decay of the transient outburst when type II bursts commence, as signalled by the presence of very energetic, flat-topped and long type II bursts (Guerriero et al. 1999). Furthermore, the double-peaked bursts are coincident with a special location in the CCD – the vertex where the source transits between the banana and the island state, indicating a change in the accretion-flow geometry (van der Klis 2006).

The non-burst light curve also shows a peculiar feature, around the double-peaked bursts: a QPO with a typical frequency of

about 0.25 Hz. This QPO is present before and after the bursts, and during the second peak of the bursts. The amplitude peaks at 5.03 ± 1.47 per cent fractional rms. Notably, it is absent during the first burst peak and the deep dips. It remains visible during shallow dips with a smaller amplitude. When compared to other type I bursts from the RB and considering the depth of the deepest dips, this strongly suggests that the QPO represents an additional radiation component to the burst and the persistent emission.

We searched all *RXTE* data on the RB and found a total of five statistically significant detections (see Section 3.3). The feature is present in all the consecutive power spectra that make up each observation and it also always lies in the same portion of the CCD across five different outbursts, at the transition between the island and banana states. Furthermore, all the observations featuring the 0.25 Hz QPO coincide with either double-peaked bursts or the kind of type II bursts (long, bright, flat-topped) which only appear in a short-lived phase of an outburst decay (Guerriero et al. 1999).

The observations of mid-burst dips during type-I X-ray bursts and the simultaneous behaviour of the 0.25 Hz QPO at a state transition are unique. How do they come about and how are they related to each other? Why do they take place during a state transition? Are they related to the unique type II bursting behaviour of the RB and, if so, can they provide us further constraints on the origin of that behaviour?

4.2 Nature of the dips

Other LMXBs exhibit double-peaked bursts that are not due to PRE. For example 4U 1636−53 shows bursts with two (Sztajno et al. 1985; Bhattacharyya & Strohmayer 2006a,b) and even three peaks (van Paradijs et al. 1986; Zhang et al. 2009). However, the time-scales for this source are different than for the RB (the peaks are separated by at most 5 s) and the flux never drops below the pre-burst emission. The similarities are that the peak flux is also a factor of 2 to 3 below the Eddington limit, the inferred mass accretion rate is relatively large and the bursts concentrate around the vertex of the island/banana branch of the CCD. Non-PRE double-peaked type I bursts have also been observed from 4U 1608−52 (Penninx et al. 1989), GX 17+2 (Kuulkers et al. 2002) and 4U 1709−267 (Jonker et al. 2004), all with durations shorter than 20 s.

There is great diversity in the observations of other sources, precluding a single explanation for all irregularities. The double-peaked bursts in the RB are no exception: they too are unique, particularly because of relatively long time-scales for the dip ingress and egress and the simultaneous QPO behaviour. We will now discuss several explanations for the double-peaks phenomenon in the other sources.

4.2.1 Two-stage energy release on the surface?

One possibility is that the multiple peaks are the result of a variation in either the rate at which the energy is transported to the surface of the NS, or in the rate at which energy is released in the flash. A shear instability could mix layers which have undergone a thermonuclear flash with unburnt material lying above them (Fujimoto et al. 1988), or there could be a waiting point in the rp-processes (Fisker, Thielemann & Wiescher 2004). However, it is difficult to keep unburnt fuel above burnt material without the two mixing (Spitkovsky, Levin & Ushomirsky 2002), or to have the burning reaction chain stalling as long as the dips are sometimes observed to last (Bhattacharyya & Strohmayer 2006a).

Other explanations discussed in literature involve stalling of the burning front. For a weak burst with high-latitude ignition, the spreading of the flame could stall at the equator if that is where most of the disc material is accreted (Bhattacharyya & Strohmayer 2006a). Otherwise, a temporary boosting of the magnetic field B, due to the motion of the fluid upon ignition, could temporarily confine the burning region (Cavecchi et al. 2011). Obviously B is not expected to be different for the double-peaked bursts and the rest of the RB bursts, nor is the fuel composition, given their similar time-scales and energetics. The ignition location and the mass-accretion rate are therefore the remaining possible triggers for a confining mechanism that could give rise to the double peaks. Perhaps high-latitude ignition could be rare enough to only happen in six bursts out of 125, although these are not among the weakest in the sample as observed for double-peaked bursts in 4U 1636−53 (Bhattacharyya & Strohmayer 2006a). On the other hand, the possibility of magnetic confinement is at odds with the fact that the RB double-peaked bursts occur in a limited range of intermediate mass-accretion rates, with single-peaked bursts being observed at both higher and lower $\dot{M}$.

4.2.2 Transient obscuration from the disc?

Generally speaking, all the scenarios discussed above revolve around phenomena confined to the surface. None of them can therefore explain why, in bursts 35 and 36, the flux drops below pre-burst levels while the absorption column density increases. The accretion flow, responsible for the non-burst emission, must clearly also be affected.

For example, the multipeaked structure could result from scattering of the X-rays by material evaporated from the accretion disc during the flash, forming a burst-induced accretion disc corona. Models seem however to require Eddington-limited bursts (Melia & Zylstra 1992), and indeed observations of radiative or dynamical interactions with the accretion disc have so far been limited to very energetic PRE bursts (in't Zand, Galloway & Ballantyne 2011; in't Zand et al. 2013; Degenaar et al. 2013). Instead, the double-peaked bursts in the RB are sub-Eddington by at least a factor of 2, implying that the burst flux delivers insufficient radiation pressure to influence the accretion flow. Even resorting to beaming, to raise the flux in a direction outside the line of sight to a sufficient level, the problem remains that the time-scales are dynamical in nature and much shorter than those observed (e.g. Melia & Zylstra 1992).

The energetic properties of these bursts are unremarkable with respect to the rest of the type I sample, which makes explaining their exceptionality difficult. None the less, the dips seem to be initiated by the bursts, responding to the burst with a delay of about 10 s. As a way around this, the origin of the dips might lie in a short-lived, peculiar geometry of the inner accretion flow rather than in the bursts themselves.

For a scenario that is independent of burst properties and features longer dips, one can look at dipping sources. These show periodic dips in their light curves that are thought to be caused by periodic obscuration of the central source by a structure formed in an interplay between the gas stream from the companion and the accretion disc (White & Swank 1982). Therefore, they have generally been inferred to be at inclination angles larger than 60° (Frank, King & Lasota 1987), unless the splash traverses over the compact object to the other side of the accretion disc (e.g., Armitage & Livio 1998).

The depth, duration and spectral properties of the dips vary from source to source and from cycle to cycle (Parmar & White 1988). The time-scale of the dips in the RB is similar to that shown by some dipping sources (e.g. Kitamoto et al. 1984), and, as we said, the fact that the dips go twice below the pre-burst flux indicates that, as in dipping sources, the persistent emission is also partially obscured.

Most importantly, the RB dips spectrum is consistent with a larger portion of the flow coming in the line of sight. Unlike in all other sources, however, in the RB the dips only occur during bursts. Likely this means that the inclination angle is lower, since at a high-inclination angle dips in the persistent emission should also be visible.

None the less, obscuration phenomena of the surface might be possible even at low inclinations. 3D MHD simulations by Romanova, Kulkarni & Lovelace (2008); Romanova et al. (2012) and Kulkarni & Romanova (2008) showed that two different regimes of accretion on magnetized stars like AMXPs are possible in presence of a tilt ($\lesssim 30°$) between the rotational axis and the magnetic dipole. At large $\dot{M}$, in what they call the 'boundary layer' regime, matter can accrete directly through the magnetosphere via narrow and tall 'tongues' due to Raleigh–Taylor instability, forming a belt-shaped hot region on the surface of the star. Instead at lower $\dot{M}$, in the so-called 'magnetospheric regime', the accretion flow forms few (two or four) ordered funnel streams towards the magnetic poles.

If these predictions are correct, for a low inclination the appearance of obscuring funnels is indeed to be expected as $\dot{M}$ goes down. Furthermore, as these funnels are nothing but transient accretion episodes at low $\dot{M}$, they might help explain the onset of the type II burst activity at the transition from the soft to the hard state. However, if this change in geometry is behind the obscuration, it remains unclear why double peaks would not be an overall characteristic of all bursts in the low $\dot{M}$ state, and also whether the a burst–funnel interaction could reproduce the observed dip durations.

4.3 Nature of 0.25 Hz QPO

QPOs in LMXBs, no matter how difficult to explain, are always ascribed to a phenomenon in the accretion flow (see van der Klis 2006, and references therein). The only exceptions are mHz QPOs which are thought to be due to marginal nuclear burning on the NS surface (Revnivtsev et al. 2001; Heger, Cumming & Woosley 2007). However, those QPOs are interrupted by type I X-ray bursts (Altamirano et al. 2008) and have frequencies one to two orders of magnitude smaller than the 0.25 Hz QPOs in the RB. Thus, it is most likely that the dipping behaviour and the 0.25 Hz QPO in the RB are related to the accretion flow.

We explore in this section two possible scenarios to explain the QPO: periodic obscurations and modulation of the accretion flow via interactions between the disc and the magnetosphere.

4.3.1 QPOs in dipping sources

At least three dipping bursting LMXBs (XB 1323−619, Jonker, van der Klis & Wijnands 1999; EXO 0748−676, Homan et al. 1999; and 4U 1746−37, Jonker et al. 2000) show ∼1 Hz QPOs. Their rms amplitudes are about 10 per cent, and the energy dependence of the rms amplitude is nearly flat. The fractional rms amplitude was found to be consistent with being constant during the persistent emission, the X-ray dips and, most importantly, type I X-ray bursts. The fact that the ∼1 Hz QPOs persist during a dip with unchanged rms indicates that they are formed in a region at a smaller radius than that where the obscuration takes place.

It seems therefore likely that the ∼1 Hz QPOs detected in dipping LMXBs are caused by matter periodically obscuring our line of sight to the NS, perhaps due to Lense–Thirring precession of a tilted inner accretion disc around a compact object (Homan 2012). Despite the rough match in frequency and amplitude, no dips have ever been observed in the persistent emission of the RB outside a burst, which

seems at odds with a system viewed at a high inclination. Also, the ∼1 Hz QPOs of dipping sources span a much larger range of accretion states, whereas the QPO in the RB appears to be confined to the transition between the island and banana states. Therefore, we consider this scenario not likely to explain the 0.25 Hz QPO in the RB.

4.3.2 QPOs from disc–magnetosphere interactions

First reported by van der Klis et al. (2000), the 1 Hz QPO that is observed in the final stages of the outbursts of SAX J1808.4−3658 was extensively studied by Patruno et al. (2009). They report a QPO frequency in the (0.8–1.6) Hz range, and an rms amplitude that grows monotonically with energy up to about 17 keV. A 1 Hz QPO of similar properties has been reported from NGC 6440 X-2 by Patruno & D'Angelo (2013), who suggest this feature has the same origin in both these AMXPs.

The most likely origin for the QPO is an accretion flow instability arising at the inner edge of the disc (Patruno et al. 2009). Among the variety of mechanisms at hand, the most promising seems to be the one first proposed by Spruit & Taam (1993) and further explored by D'Angelo & Spruit (2010, 2012). In this model, an instability can develop when the magnetosphere truncates the inner accretion disc at a radius r_{in} that is outside but still close to the corotation radius r_{cor}. A new disc solution known as 'dead disc' is then found (Sunyaev & Shakura 1977; D'Angelo & Spruit 2010, 2012) which is alternative to the 'propeller' regime (Illarionov & Sunyaev 1975), where the transfer of angular momentum effectively expels matter from the system, and the inner disc radius keeps increasing as $\dot{M}$ decreases. When $r_{in} \gtrsim r_{cor}$, the transfer of angular momentum happens from the NS to the disc, spinning down the NS and changing the radial gas density distribution at the inner disc region without matter expulsion. In a dead disc, r_{in} does not evolve far from r_{cor} and the matter keeps flowing in from the outer disc regions piling up there. If certain conditions are met at the magnetosphere–disc interaction (D'Angelo & Spruit 2010, 2012) a critical pressure is eventually reached under which the gas slips inside r_{cor}, thereby initiating a sudden accretion event. After that, the accumulated mass reservoir is depleted, and a new cycle begins.

This instability is a potentially interesting model for the 0.25 Hz QPO in the RB. The frequency of the instability depends on the viscous time-scale at the inner disc edge, which in turn depends on the mass accretion rate and on the location of the inner disc (see e.g. equation 9 in Patruno & D'Angelo 2013). Unfortunately, the inner disc radius is not known for the RB, since neither the spin frequency of the NS nor the strength of its magnetic dipole are known.

Also, a slightly growing rms-E relation is observed in the RB, which is also observed in the other two sources. While the increase is weaker than in SAX J1808.4−3658 or NGC 6440 X-2, this can be explained with the smaller fractional amplitude of the QPO in the RB. Patruno & D'Angelo (2013) explain the monotonic increase in rms with energy in SAX J1808.4−3658 and NGC 6440 X-2 arguing that as the instability is caused by changes in $\dot{M}$, and the latter change the density and temperature of the corona where the photons are upscattered, the QPO fluctuations will translate to a varying hardness of the spectrum, making the high-energy flux more variable than the low-energy one. In case of a strong persistent emission, as is the case in the RB, the effect will obviously be weaker.

Differences are, however, clearly present. The QPO in the two AMXPs cannot be fitted with a Lorentzian because of its fast decline in power at low frequencies. This is however not seen in the

RB QPO. Furthermore, the rms amplitude of the QPO is more than one order of magnitude larger in the two other sources than in the RB. This is because nearly no accretion takes place during the QPO minima in SAX J1808.4−3658 and NGC 6440 X-2, which show the oscillation at moderately low luminosities. The higher count rates and the different QPO shape observed in the RB are therefore challenging to this scenario. Even though the results from D'Angelo & Spruit (2010) show that for certain ranges of parameters accretion can in fact continue to take place in the minima of the QPO, the instability is predicted to produce a much larger modulation of the mass accretion rate $\dot{M}$ than observed in the RB, when at the time of the double-peaked bursts $\dot{M} \simeq 4 \times 10^{-9}\,\mathrm{M}_{\odot}\,\mathrm{yr}^{-1}$, roughly one order of magnitude larger than what observed in the two other sources at the time of the appearance of the QPO there.

If however we again invoke a two-channel accretion (see Section 4.2), with a polar and an equatorial channels, one controlled by the instability and the other one unaffected by it, the lower amplitude would naturally follow. For example, while the centrifugal barrier could act to modulate the equatorial accretion, matter could be leaking from above and below it, and accrete along the B lines.

Also involving two-channel accretion, the disc–magnetospheric interactions described in Romanova et al. (2008) and Kulkarni & Romanova (2008) can as well explain the appearance of periodicities in the light curve, via accretion-induced hotspots. While at high $\dot{M}$ sporadically forming 'tongues' hit the star in random places, so that the light curve is irregular, at low $\dot{M}$ the funnels driving matter from the disc to the magnetic poles are relatively stable, so that the position of the hot spots is almost constant, resulting in a modulation of the light curve. Again, the problem with this model is that it does not explain why the QPO is short-lived, rather than being an overall characteristic of the island state.

4.4 Linking the dips and the QPO

In Table 3, we list the possible scenarios for the dips and the QPO, and which relevant observables they are capable of explaining.

The only model that is not ruled out by any observable involves a relatively short-lived accretion state consisting of two different accretion channels, an equatorial and a polar one, in a system viewed at low inclination. As part of the inner accretion flow in this particular state goes along the magnetic field lines to the NS poles, it is then easier for material to come in the line of sight if the inclination

angle is low, and for the burst to disturb the accretion flow, thereby causing the flux to dip below the pre-burst level, even if the burst flux is sub-Eddington.

Since the 0.25 Hz QPO disappears during some of the dips, its place of origin would also seem to be obscured by the same material. This suggests that the QPO originates close to the NS and closer than the X-ray emitting part of the accretion disc. The latter region probably reaches out to 10^4 km (Mitsuda et al. 1984; Makishima et al. 1986), so the obscuring material would have to be substantially closer than that. If the QPO originates in the equatorial flow, the accretion channel along the magnetic field could be disturbed by the burst so that, given the low inclination, the radiation from the NS surface and the equatorial flow would be obscured, making the dips deeper than the pre-burst emission and causing the temporary disappearance of the QPO. If instead the QPO originates in the disrupted polar flow, its disappearance at the time when the dips are deeper than the pre-burst emission would still naturally follow.

To match the observations, this peculiar configuration should be short-lived, appearing roughly at the same time when the type II burst do, and disappearing within days. It is generally thought that in the banana state, at larger mass-accretion rates, a geometrically thin and optically thick disc probably extends down to very close to the NS surface, whereas the lack of dips in the island state, at lower mass-accretion rates, could be due to a quasi-spherically symmetric accretion via an optically thin corona (see e.g. review by Done, Gierliński & Kubota 2007). The rarity of the double-peaked bursts and of the 0.25 Hz QPO would then match the fact that they occur in a particular accretion state of the RB, when part of the accretion flow is starting to become diverted to the type II bursting mechanism.

5 CONCLUSIONS

We have reported the coincident observation of non-PRE, double-peaked type I bursts and an LF QPO with a frequency of about 0.25 Hz. They occur at the transition from the banana to the island state, when the geometry of the accretion flow is expected to change. This transition also coincides with the appearance of type II bursts. Despite being sometimes at roughly the same count rate as the pre-burst persistent emission, the dip between the two peaks has a distinctively different spectrum, with a much larger hydrogen column density required to fit the data. This is suggestive of some kind of temporary obscuration of the NS surface. Also, the dips in

Table 3. Mechanisms for the dips and QPO.

Model	Bursts			QPO			Accretion state	
	Double peaks [a]	$\Delta t_{\mathrm{dip}}^{[b]}$	Spectrum[c]	ν_0	rms	rms/Energy[d]	Soft/Hard[e]	Type II burst[f]
Unburnt layer	Y	P	N	–	–	–	–	–
Reaction chain stalling	Y	N	N	–	–	–	–	–
Equatorial stalling	Y	P	N	–	–	–	P	–
Magnetic confinement	Y	P	N	–	–	–	N	–
Burst-induced corona	N	N	Y	–	–	–	–	–
Marginally stable burning	–	–	–	N	Y	N	Y	–
High inclination (dipper)	Y	Y	Y	Y	Y	N	N	–
Disc-magnetosphere instability	–	–	–	Y	N	Y	N	Y
Low inclination, two channels	Y	P	Y	P	–	–	Y	P

The table compares the properties of the bursts, the QPO and the source state against the predictions made by the various models discussed in Section 4. Y/N (yes/no) indicates that the model can/cannot explain the property in a given column. The symbol P (possible) indicates that the model might be able to explain the property if certain conditions are met. An empty field indicates that the model makes no specific prediction for that property. [a]Non-PRE, double-peaked bursts; [b]dip duration; [c]enhanced absorption in the dip spectrum and dip going below the persistent flux level; [d]QPO fractional amplitude growing with energy; [e]appearance of the dip and the QPO only at the soft/hard transition; [f]appearance of the dip and QPO at the same time as the first type II bursts.

two bursts go below the pre-burst emission level, meaning part of the accretion flow is also obscured, or perhaps even disrupted. No dips are ever observed in the persistent emission outside a burst.

We have explored several models to explain the dips, the QPO, and the peculiar accretion state in which they appear, including confining mechanisms on the NS surface, obscuration of the surface and inner accretion flow in a high-inclination system, and accretion instabilities borne out of the interaction between the accretion disc and the magnetosphere.

Although no single model can explain all the observables, we favour a two-channel accretion state, transitional between the soft and hard state. Mass accretion on to the magnetic poles would allow for the burst to disturb the accretion flow even if the burst flux is sub-Eddington. If the source is viewed at a low inclination, the temporary disruption of the polar accretion channel by the burst could then obscure the NS surface, which would cause the flux to go below its pre-burst level, and in some cases even the inner equatorial accretion flow. If the instability causing the QPO controlled the equatorial channel, the disappearance of the QPO in the deepest dips could also be explained.

Furthermore, investigation is necessary to develop this model beyond this qualitative picture. It remains to be seen whether such an accretion geometry could indeed be sustainable, confined to a very narrow range of accretion rates, and whether this scenario could reproduce the fairly long dips. The difficulty of constraining such a model notwithstanding, the obscuration that is responsible from the dip must be connected with the disc instability that is responsible for the QPO and the type II bursts.

REFERENCES

Altamirano D., van der Klis M., Wijnands R., Cumming A., 2008, ApJ, 673, L35

Armitage P. J., Livio M., 1998, ApJ, 493, 898

Baan W. A., 1977, ApJ, 214, 245

Baan W. A., 1979, ApJ, 227, 987

Bagnoli T., in't Zand J. J. M., Galloway D. K., Watts A. L., 2013, MNRAS, 431, 1947 (B13)

Belloni T., Psaltis D., van der Klis M., 2002, ApJ, 572, 392

Bhattacharyya S., Strohmayer T. E., 2006a, ApJ, 636, L121

Bhattacharyya S., Strohmayer T. E., 2006b, ApJ, 641, L53

Cavecchi Y. et al., 2011, ApJ, 740, L8

Cornelisse R. et al., 2003, A&A, 405, 1033

D'Angelo C. R., Spruit H. C., 2010, MNRAS, 406, 1208

D'Angelo C. R., Spruit H. C., 2012, MNRAS, 420, 416

Degenaar N., Miller J. M., Wijnands R., Altamirano D., Fabian A. C., 2013, ApJ, 767, L37

Done C., Gierliński M., Kubota A., 2007, A&AR, 15, 1

Egron E. et al., 2011, A&A, 530, A99

Falanga M., Farinelli R., Goldoni P., Frontera F., Goldwurm A., Stella L., 2004, A&A, 426, 979

Fisker J. L., Thielemann F.-K., Wiescher M., 2004, ApJ, 608, L61

Fox D., Smith D., Lewin W., Rutledge R., 1998, Astron. Telegram, 32, 1

Fox D. W. et al., 2001, MNRAS, 321, 776

Frank J., King A. R., Lasota J.-P., 1987, A&A, 178, 137

Frogel J. A., Kuchinski L. E., Tiede G. P., 1995, AJ, 109, 1154

Fujimoto M. Y., Sztajno M., Lewin W. H. G., van Paradijs J., 1988, A&A, 199, L9

Galloway D. K., Muno M. P., Hartman J. M., Psaltis D., Chakrabarty D., 2008, ApJS, 179, 360

Guerriero R. et al., 1999, MNRAS, 307, 179

Hasinger G., van der Klis M., 1989, A&A, 225, 79

Heger A., Cumming A., Woosley S. E., 2007, ApJ, 665, 1311

Hoffman J. A., Marshall H. L., Lewin W. H. G., 1978, Nature, 271, 630

Homan J., 2012, ApJ, 760, L30

Homan J., Jonker P. G., Wijnands R., van der Klis M., van Paradijs J., 1999, ApJ, 516, L91

Homan J. et al., 2010, ApJ, 719, 201

Illarionov A. F., Sunyaev R. A., 1975, A&A, 39, 185

in't Zand J. J. M., Galloway D. K., Ballantyne D. R., 2011, A&A, 525, A111

in't Zand J. J. M. et al., 2013, A&A, 553, A83

Jahoda K., Markwardt C. B., Radeva Y., Rots A. H., Stark M. J., Swank J. H., Strohmayer T. E., Zhang W., 2006, ApJS, 163, 401

Jonker P. G., van der Klis M., Wijnands R., 1999, ApJ, 511, L41

Jonker P. G., van der Klis M., Homan J., Wijnands R., van Paradijs J., Méndez M., Kuulkers E., Ford E. C., 2000, ApJ, 531, 453

Jonker P. G., Galloway D. K., McClintock J. E., Buxton M., Garcia M., Murray S., 2004, MNRAS, 354, 666

Kitamoto S., Miyamoto S., Tanaka Y., Ohashi T., Kondo Y., Tawara Y., Nakagawa M., 1984, PASJ, 36, 731

Klein-Wolt M., Homan J., van der Klis M., 2004, Nucl. Phys. B, 132, 381

Kouveliotou C., van Paradijs J., Fishman G. J., Briggs M. S., Kommers J., Harmon B. A., Meegan C. A., Lewin W. H. G., 1996, Nature, 379, 799

Kubota A., Tanaka Y., Makishima K., Ueda Y., Dotani T., Inoue H., Yamaoka K., 1998, PASJ, 50, 667

Kulkarni A. K., Romanova M. M., 2008, MNRAS, 386, 673

Kuulkers E., Homan J., van der Klis M., Lewin W. H. G., Méndez M., 2002, A&A, 382, 947

Lamb F. K., Fabian A. C., Pringle J. E., Lamb D. Q., 1977, ApJ, 217, 197

Levine A. M., Bradt H., Cui W., Jernigan J. G., Morgan E. H., Remillard R., Shirey R. E., Smith D. A., 1996, ApJ, 469, L33

Lewin W. H. G., van Paradijs J., Taam R. E., 1993, Space Sci. Rev., 62, 223

Linares M., Altamirano D., Chakrabarty D., Cumming A., Keek L., 2012, ApJ, 748, 82

Lubin L. M., Lewin W. H. G., Rutledge R. E., van Paradijs J., van der Klis M., Stella L., 1992, MNRAS, 258, 759

Makishima K., Maejima Y., Mitsuda K., Bradt H. V., Remillard R. A., Tuohy I. R., Hoshi R., Nakagawa M., 1986, ApJ, 308, 635

Masetti N., 2002, A&A, 381, L45

Masetti N. et al., 2000, A&A, 363, 188

Melia F., Zylstra G. J., 1992, ApJ, 398, L53

Mitsuda K. et al., 1984, PASJ, 36, 741

Morrison R., McCammon D., 1983, ApJ, 270, 119

Parmar A. N., White N. E., 1988, J. Ital. Astron. Soc., 59, 147

Patruno A., D'Angelo C., 2013, ApJ, 771, 94

Patruno A., Watts A., Klein Wolt M., Wijnands R., van der Klis M., 2009, ApJ, 707, 1296

Penninx W., Damen E., van Paradijs J., Tan J., Lewin W. H. G., 1989, A&A, 208, 146

Revnivtsev M., Churazov E., Gilfanov M., Sunyaev R., 2001, A&A, 372, 138

Romanova M. M., Kulkarni A. K., Lovelace R. V. E., 2008, ApJ, 673, L171

Romanova M. M., Ustyugova G. V., Koldoba A. V., Lovelace R. V. E., 2012, MNRAS, 421, 63

Rutledge R. E., Lubin L. M., Lewin W. H. G., Vaughan B., van Paradijs J., van der Klis M., 1995, MNRAS, 277, 523

Spitkovsky A., Levin Y., Ushomirsky G., 2002, ApJ, 566, 1018

Spruit H. C., Taam R. E., 1993, ApJ, 402, 593

Stella L., Haberl F., Lewin W. H. G., Parmar A. N., van Paradijs J., White N. E., 1988, ApJ, 324, 379

Strohmayer T., Bildsten L., 2006, in Lewin W. H. G., van der Klis M., eds, New Views of Thermonuclear Bursts. Cambridge Univ. Press, Cambridge, p. 113

Sunyaev R. A., Shakura N. I., 1977, Sov. Astron. Lett., 3, 138

Sztajno M., van Paradijs J., Lewin W. H. G., Trumper J., Stollman G., Pietsch W., van der Klis M., 1985, ApJ, 299, 487

Valenti E., Ferraro F. R., Origlia L., 2010, MNRAS, 402, 1729

van der Klis M., 1995, in Alpar M. A., Kiziloglu U., van Paradijs J., eds, The Lives of the Neutron Stars Rapid Variability in X-ray Binaries - Toward a Unified Description. Kluwer, Dordrecht, p. 301

van der Klis M., 2006, in Lewin W., van der Klis M., eds, Rapid X-ray Variability. Cambridge Univ. Press, Cambridge, p. 39

van der Klis M., Chakrabarty D., Lee J. C., Morgan E. H., Wijnands R., Markwardt C. B., Swank J. H., 2000, IAU Circ., 7358, 3

van Paradijs J., Sztajno M., Lewin W. H. G., Trumper J., Vacca W. D., van der Klis M., 1986, MNRAS, 221, 617

van Straaten S., van der Klis M., Méndez M., 2003, ApJ, 596, 1155

Watts A. L., 2012, ARA&A, 50, 609

White N. E., Swank J. H., 1982, ApJ, 253, L61

Worpel H., Galloway D. K., Price D. J., 2013, ApJ, 772, 94

Zhang W., Jahoda K., Swank J. H., Morgan E. H., Giles A. B., 1995, ApJ, 449, 930

Zhang G., Méndez M., Altamirano D., Belloni T. M., Homan J., 2009, MNRAS, 398, 368

This paper has been typeset from a TEX/LATEX file prepared by the author.